RESEARCH ARTICLE | DECEMBER 13 2018

Vortex fibers for STED microscopy

Special Collection: Intermodal and Multimode Fiber Photonics

Lu Yan ; Poul Kristensen; Siddharth Ramachandran

APL Photonics 4, 022903 (2019)
https://doi.org/10.1063/1.5045233
CHORUS

Vortex fibers for STED microscopy

Cite as: APL Photonics 4, 022903 (2019); doi: 10.1063/1.5045233
Submitted: 18 June 2018 • Accepted: 28 August 2018 •
Published Online: 13 December 2018

Lu Yan,[1,a)] Poul Kristensen,[2] and Siddharth Ramachandran[1,b)]

AFFILIATIONS

[1] Department of Electrical and Computer Engineering, Boston University, 8 St. Mary's St., Boston, Massachusetts 02215, USA
[2] OFS-Fitel, Priorparken 680, Brøndby 2605, Denmark

[a)] Currently at Applied Materials, Inc., 3340 Scott Blvd., Santa Clara, California 95054, USA
[b)] Author to whom correspondence should be addressed: sidr@bu.edu

ABSTRACT

Super-resolution imaging using the principles of stimulated emission depletion (STED) microscopy requires collinear excitation of a sample with a Gaussian-shaped excitation beam and a donut-shaped depletion beam whose spin (polarization) and orbital angular momentum (OAM) signs are aligned. We leverage recent advances in stable OAM mode propagation in optical fibers for telecom applications to design, fabricate, and validate the utility of a vortex fiber as the beam shaping device at visible and near-IR wavelengths for STED microscopy. Specifically, using compact UV-written fiber-gratings yielding high purity mode conversion (98.7%), we demonstrate the simultaneous generation of Gaussian and OAM beams at user-defined wavelengths. Point spread function measurements reveal a depletion beam with >17.5-dB extinction ratio, a naturally co-aligned Gaussian beam, and a setup in which these characteristics are maintained even as the fiber is bent down 6-mm radii. The proof-of-concept of all-fiber STED microscopy realized using this fiber device is used to image fluorescent bead samples yielding a sub-diffraction-limited resolution of 103 nm in the lateral plane. This opens the door to performing fiber-based STED microscopy with a setup that is not only resistant to environmental perturbations but also facilitates the development of endoscopic STED imaging.

Stimulated emission depletion (STED) microscopy[1] is a highly attractive super-resolution imaging technique because it operates in the far-field and hence leverages advances in confocal microscopy such as ease of use and speed of image acquisition. It employs Gaussian beams for excitation, and modes carrying orbital angular momentum (OAM) as depletion beams, and is one of the most successful applications of the class of cylindrical vector modes that have gained extensive recent attention.[2] Over the past decade, breakthroughs in laser sources, fluorescence probes, depletion schemes, and detection techniques have dramatically advanced the field of STED microscopy, and sub-50 nm resolution can now be routinely obtained.[3] Despite the aforementioned developments, several current implementations of STED[4–8] use free-space beam shaping devices for achieving Gaussian and OAM beams at the desired colors. This usually requires precise co-alignment of two or more spatially and spectrally distinct laser beams. Additional polarization control is typically needed to obtain a depletion pattern with sufficiently low central intensity at the focal plane of a high numerical aperture (NA) objective. A fiber based alternative that can provide the desired optical functionalities, on the other hand, would potentially yield lower-loss, more compact, reliable, and otherwise more robust systems facilitating widespread adoption. Realization of a robust all-fiber STED microscope could also potentially facilitate endoscopic implementation of the STED technique, allowing access to sub-cellular structures at larger penetration depth and during chronic experiments that are required for *in vivo* super-resolution imaging.

Several fiber based implementations of STED have been attempted to date: OAM generation at the output of an optical fiber may be achieved via excitation of multiple optical modes in a fiber, which when combined with the appropriate phase differences, yields an interference pattern at the output representing a beam carrying OAM.[9–12] Unfortunately, the desired OAM output, being formed via multimode interference, is, by definition, not inherently stable, implying that the constituent fiber cannot be bent, perturbed, or otherwise deployed as a flexible probe. Alternatively, one solution to this modal instability problem is to maximize the group-delay difference of the

constituent modes that form the desired interference pattern. Then, for sufficiently broadband light with a coherence time lower than the group-delay difference between the modes, a stable output is obtained.[13]

Here, we demonstrate an all-fiber based device that satisfies all the requirements for STED microscopy without inherent operation wavelength or bandwidth limitations, while providing significantly higher tolerances to environmental perturbations than those that can be withstood by a free-space STED microscopy system. The critical enabler in our demonstration is the design and development of an optical fiber that supports stable OAM mode propagation at the visible and near-IR wavelengths that are typically used in STED. This is combined with well-established fiber-grating technology to realize compact (3.1-cm long) mode converters that yield high purity (>99.7%) OAM beams at the depletion wavelength, and Gaussian beams at other wavelengths, thereby yielding a naturally self-aligned system producing the desired beams for STED. Being an all-fiber device in nature, the insertion loss of the entire device is also low (<1 dB). We characterize the device by testing the resultant point-spread function (PSF) using a home-built confocal microscope and find that the donut beam extinction ratio under high-NA focusing is greater than 17.5 dB, which is ~4.5 dB greater than that typically required.[4] We then build an all-fiber STED microscope using the device and demonstrate a sub-diffraction-limited lateral resolution of 103 nm by imaging fluorescent bead samples, corresponding to an ~4-fold improvement compared to the confocal imaging results obtained with the same setup. The benefit of the all-fiber construction is illustrated by the fact that the aforementioned attributes are maintained even as we strongly perturb the fiber, including with 10 fiber loops of bend radii as small as 6 mm—perturbations substantially exceeding even those encountered by fibers in endoscope configurations.

In waveguides with cylindrical symmetry, the first group of higher order modes (HOMs) $TE_{0,1}$, OAM ($L = \pm 1$), and $TM_{0,1}$ are eigensolutions to the vectorial Helmholtz equation.[14] In conventional optical fibers, the effective index differences, Δn_{eff}, between these modes are $\lesssim 10^{-5}$; hence, even minor bend perturbations couple these modes, making OAM mode delivery hard, if not impossible. It is now well known that appropriately designed ring-core refractive index profiles can help alleviate this mode instability problem and designs with a central core and a ring of high refractive index,[15] inverse parabolic index profiles,[16] helicoidal microstructures,[17] and ring index air core profiles[18] have been demonstrated to offer stable OAM state propagation in optical fibers in the telecom wavelength range. The same design methodology could, in principle, be used to realize optical fibers that can stably propagate OAM $-L- = 1$ modes in the visible and near-IR wavelength ranges where STED is employed. However, unlike in telecom applications, where only stable modes are needed for encoding data in mode-division multiplexing schemes,[19] STED microscopy with fiber modes also requires the design to be constrained by mode shape—namely, that the fundamental mode be substantially Gaussian-shaped and that the OAM mode be substantially single-ring donut-shaped. While the latter is generally easier to achieve, the fundamental mode can substantially depart from a Gaussian shape, especially in fibers that have high refractive index rings.

Figure 1(a) shows the experimentally measured refractive index profile of an optical fiber we designed and fabricated for STED applications. Due to the small dimensions of the index features, our commercial index profiler (IFA-100; InterFiber Analysis) is not able to revolve the waveguide, so we, instead, measure the preform from which the fiber was drawn and scale dimensions to match that of our fiber (with outer dimension OD = 125 μm). Figure 1(b) is the microscope image of the cleaved fiber, the zoomed-in version of which (see the inset) reveals the high index ring structure of this design. We use a home-built vector mode-solver[20] and the profile of Fig. 1(a) to numerically simulate the properties of this fiber.

The simulated effective index indicates a cutoff wavelength of ~930 nm [Fig. 2(a)] for the 1st HOM group, which, being far from the operational spectral range (500-800 nm), gives us confidence that OAM modes would be well-guided and not susceptible to macrobend losses. The simulated Δn_{eff} between the OAM modes and their adjacent modes is $>1 \times 10^{-4}$ at the STED wavelength of 776 nm [Fig. 2(b)]. Previous investigations of OAM modes in fibers indicate that this Δn_{eff} value suffices to inhibit coherent coupling (and hence instability) between adjacent modes.[15]

A practical fiber design must also facilitate the incorporation of a robust mode conversion technology that enables converting the incoming Gaussian-shaped laser beam at the

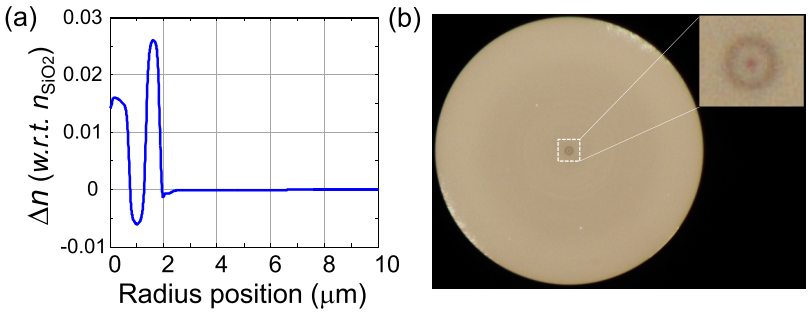

FIG. 1. (a) Measured refractive index profile of the preform scaled to OD 125 μm. (b) Microscope image of the cleaved facet of an OD 125 μm vortex fiber. Inset: zoomed-in image. Scale bar: 10 μm.

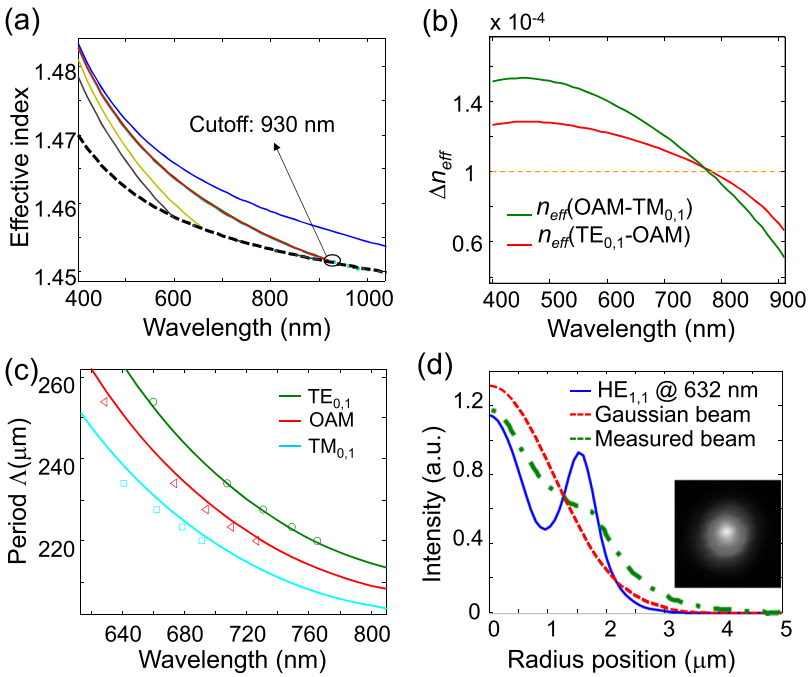

FIG. 2. Simulated results for OD 125 μm vortex fiber: (a) effective index, n_{eff}, and (b) effective index differences, Δn_{eff}, as a function of wavelength. The dashed line shows the design threshold of 10^{-4} for Δn_{eff}; (c) grating phase matching curves. The markers represent the experimental LPG data. (d) Intensity profiles of the fundamental mode $HE_{1,1}$ at λ_{exc} = 632 nm and an ideal Gaussian function. The inset shows an experimentally measured near-field image of the $HE_{1,1}$ mode of this fiber at 632.8 nm.

STED wavelength into an OAM beam in the fiber. While free-space techniques exist,[6,7,9,11] they would detract from our all-fiber construction, and here we wish to leverage well-established fiber-based long-period grating (LPG) technology[21] to realize in-fiber mode conversion. Figure 2(c) shows the required LPG period Λ, as a function of wavelength λ for the 1st group of HOMs, calculated from the simulated fiber parameters by $\Lambda = 1/\lambda(n_{eff}^{HE11} - n_{eff}^{HOM})$, where n_{eff}^{HE11} and n_{eff}^{HOM} are the effective indices of the fundamental and higher order modes, respectively.

Figure 2(c) predicts $\Lambda \sim 210$ μm for OAM mode conversion at 776 nm. While even shorter grating periods are achievable with the UV-inscription technique (to be described later) we employ, conversion from the fundamental mode of a fiber to these 1st higher order anti-symmetric modes may also be achieved with gratings formed via mechanical microbends,[22] acousto-optic interactions,[23] or CO_2 laser or splicer-arc induced controlled fiber deformations.[24] A subset of these latter techniques also offer tunable mode conversion of great utility to STED applications where one may wish to change wavelengths of operation. However, save for the UV-induced grating fabrication method, these other techniques primarily work only when the required period is of the same order as the fiber dimension, i.e., for $\Lambda \gtrsim 100$ μm. The fiber designs illustrated in Figs. 1 and 2 were obtained with this constraint in mind, so as to enable this fiber to be universally applicable across a range of desired wavelengths, and with a variety of mode conversion technologies.

We now turn our attention to the final design criterion—as mentioned earlier, we need a substantially Gaussian shaped fundamental mode $HE_{1,1}$ in this fiber because (1) this results in good mode matching, and hence low splice loss, with light from a single mode fiber (SMF) forming the pigtails of the device and (2) it yields close to diffraction-limited excitation spot sizes for imaging. Figure 2(d) shows the simulated intensity profile of the $HE_{1,1}$ mode of the vortex fiber shown in Fig. 1, along with the intensity profile of an appropriately sized Gaussian beam. The two profiles appear to be substantially different, but calculating the overlap integral between them, given by $\int_{A_{fiber}} \Psi_{Gau} \cdot \Psi_{HE_{11}} dA_{fiber}$ (A_{fiber}—cross-sectional area, Ψ_{Gau}—Gaussian function, $\Psi_{HE_{11}}$—fundamental mode field), yields ~93%. Hence the HE_{11} mode of this fiber is effectively Gaussian in shape. The inset shows the experimentally measured near-field image of the $HE_{1,1}$ mode at Λ = 632.8 nm. We notice that this beam, in fact, appears more Gaussian-like than the simulated one, which suggests that the actual fundamental mode of this fiber is more suitable for our applications than the simulations would suggest (confirmed with imaging measurements described later). We speculate that one of the origins of this (fortunate) discrepancy is that we used preform profiles for simulations, whereas the drawn fiber may have rounded off the sharp edges of the refractive index rings due to dopant diffusion, yielding more Gaussian-shaped intensity profiles for the fundamental mode.

A UV laser beam at 244 nm (Innova 300C MotoFreD, Coherent) with a full width at half maximum (FWHM) size of 12.4 μm is used to point-by-point inscribe tilted LPGs[25] in our vortex fiber. Prior to fabrication, the fiber is kept in a pressurized hydrogen chamber for 72 h to increase its photosensitivity. Due to the multimode nature of the fiber, characterizing the LPGs via a conventional transmission spectrum

measurement requires tapers with a waist diameter of 70 μm to strip out HOMs at the input and output of the grating. Taper fabrication involves heating the fiber with plasma arcs and pulling the two ends with a programmed velocity profile. The fabrication parameters as well as the taper diameter are chosen so that only the fundamental mode is guided in the taper region and the transition regions do not introduce extra mode coupling. A transmission spectrum of such taper devices can be used to optically characterize their performance,[26] which shows that we can obtain devices with single mode purities as high as 30 dB, which is sufficient for characterizing our grating mode converters.

A series of gratings with different periods are fabricated and characterized. The grating resonances for the 1st group of HOMs are plotted as a function of wavelength in Fig. 2(c)—note the excellent match between the experimental data and simulations. The LPG used in this study is ~31-mm long and has a period Λ = 208.5 μm.

The vortex fiber with this grating is fusion spliced to SMF. Combined losses (from the splice and grating) are 0.9 dB. This is rather high for LPG technology, which usually results in <0.1 dB losses. We determined that the majority of our losses arose from accidental coupling to higher order cladding modes—this is a solvable problem since cladding-mode spectra depend on the diameter of the fiber cladding, which can be changed to avoid them without affecting the performance of any core modes that are used for STED illumination. The inset (ii) of Fig. 3(b) shows the transmission spectrum of this grating, revealing a mode conversion efficiency of 99.7% at 776.34 nm. We use spatial interferometry ("ring technique"; see Fig. 3(a) for system schematic)[27] to analyze the mode purity by projecting the output of the fiber into two circular polarizations $\hat{\sigma}^+$ and $\hat{\sigma}^-$ using a quarter waveplate (WPQ05M-780, Thorlabs) and a polarizing beam displacer (PBD; BD40, Thorlabs). Performing spatial Fourier analysis on the azimuthal intensity profiles yields mode purities [plotted in Fig. 3(b) as a function of fiber bend radius]. Insets (i) and (iii) show the pictures of the coiled vortex fiber (top panels) and the corresponding near-field mode images (bottom panels), respectively. We confirm that, with the bending radius down to 6 mm, the mode purity for OAM modes stays—better than 19 dB (i.e., 98.7%). High mode purity is essential for STED microscopy since other modes like $TM_{0,1}$ and $HE_{1,1}$ diminish the darkness of the donut center spot at the focal plane of a high NA objective,[28] and this dramatically degrades the depletion efficiency, thus compromising resolution. Bends sharper than 6-mm radius induced significant bend loss, but this is already much tighter than the specifications for typical fiber-based microscopes or endoscopes.[29]

The experimental setup used to characterize the PSF of our device is shown in Fig. 4. The excitation (λ = 632.8 nm; HeNe, Melles Griot) and STED/depletion (λ = 776.34 nm, 3900S Ti:Sapphire, Spectra Physics) lasers are combined into an SMF pigtail using a fiberized wavelength division multiplexer (WDM; NR73A1, Thorlabs) and an in-line fiber polarization controller (polcon). The insertion losses of the WDM at 776.34 nm and 632.8 nm are measured to be 0.8 dB and 0.5 dB, respectively. Following the grating, another fiber polcon is used to control the OAM and polarization content of the output. The OAM eigenmodes in our fiber represent a pair of degenerate modes with spin polarization $\hat{\sigma}^{\pm}$ of the same sign as OAM L = ±1. While the design of this fiber eliminates coupling of the OAM modes to the parasitic TE_{01} and TM_{01} modes,

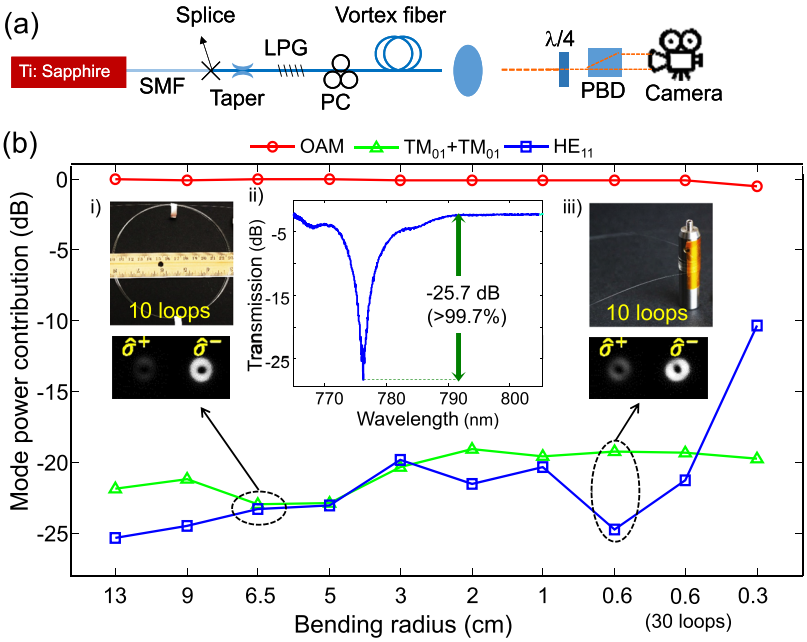

FIG. 3. (a) Setup schematic. PC: polarization controller; λ/4: quarter waveplate; PBD: polarizing beam displacer. (b) Mode purity for different bending radii. Inset: (i) and (iii) are the pictures of coiled vortex fiber together with a ruler and a ∅1/2 in. optical post, respectively (top panels), and the corresponding OAM mode images with circular polarization projections $\hat{\sigma}^+$ and $\hat{\sigma}^-$ (bottom panels); (ii) typical transmission spectrum of the UV grating showing >99.7% mode conversion efficiency.

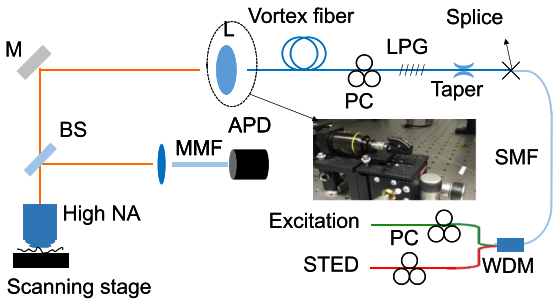

FIG. 4. System schematic. FFC: fused fiber coupler; SMF: single mode fiber; PC: polarization controller; L: lens; M: mirror; BS: beam splitter; DM: dichroic mirror; PBD: polarizing beam displacer. Inset: the photo of the clamped vortex fiber output.

coupling between these two degenerate OAM modes is possible, and controllably adjustable using polcons, in analogy with a conventional fiber polcon mixing the polarizations $\hat{\sigma}^{\pm}$ of the fundamental HE_{11} mode in SMF. Note that this polcon is used only for the purposes of characterization and is not really needed for STED operation, since either of these degenerate modes (as well as their linear combinations) yields the desired dark center spots under high NA illumination. After ~5.1 m of propagation in the vortex fiber, its output is clamped using a bare fiber adapter (BFT1, Thorlabs; see the inset in Fig. 4) for PSF measurements. The beam output is collimated using an objective lens (UPlanApo 10×, Olympus) and focused by using a high NA objective (UPlanSApo 60×/1.35, Olympus) onto a sample that is mounted on a 3-axis piezo scanning stage (NanoMax-TS, Thorlabs). Light from the sample is directed by using a free-space beam splitter (for PSF characterization) or a 2 mm thick dichroic mirror (for STED imaging; ZT670dcrb, Chroma), focused by using a tube lens (f = 300 mm; AC254-300-B-ML, Thorlabs) into a multimode fiber (MMF; M50L02S-B, Thorlabs) acting as a confocal pinhole, and detected by using an avalanche photodiode (APD; SPCM-AQR-15, Perkin Elmer). The microscopy system is controlled by a homemade LabVIEW program with a data acquisition card (PCIe-6353, National Instruments).

For bend radii of 6.5 cm and 6 mm, we measure the PSF for the excitation and STED beams, respectively, by scanning a sample of gold beads (150 nm Au nanoparticle, Cytodiagnostics). The two PSFs are spatially well aligned in both directions (Fig. 5). The FWHM of the excitation PSF is ~382 nm, and that of the dark center of the donut is ~235 nm. These values compare well with our calculations employing vectorial diffraction theory (shown with blue dashed lines) and are comparable with the corresponding characteristics of state-of-the-art free-space STED microscopy systems. The extinction ratio, defined as the ratio between intensity at the image center and that at its peak, is 18.1 dB when the fiber is coiled with a 6.5 cm radius and only slightly reduces to 17.5 dB when the fiber is tightly wound around an optical post, with a bend radius of 6 mm. These values comfortably exceed the 13-dB extinction ratio deemed as a desirable value for practical STED applications.[4]

Having characterized the PSF of the system, the all-fiber STED system is used to perform STED imaging experiments. The beam splitter in the system (Fig. 4) is replaced by a custom-made 2 mm thick dichroic mirror (ZT670dcrb, Chroma, USA). A bandpass filter (FF02-675/67-25, Semrock, USA) is placed in front of the detector to block the residual light from both the excitation and STED lasers. The vortex fiber is coiled into 6.5 cm loops on an optical table. Fluorescent microsphere (FluoSpheres DarkRed, 0.04 μm, Molecular Probes, USA) samples are prepared and imaged, with excitation and STED laser powers of 70 μW and 381 mW (maximum available from our CW laser), respectively, measured at the back aperture of the high NA objective lens. The pixel dwell time is set to 0.19 ms.

Figure 6 shows the raw images of the fluorescent beads with (a) only the excitation laser (confocal mode) and (b) both the excitation and STED lasers (STED mode) illuminating the

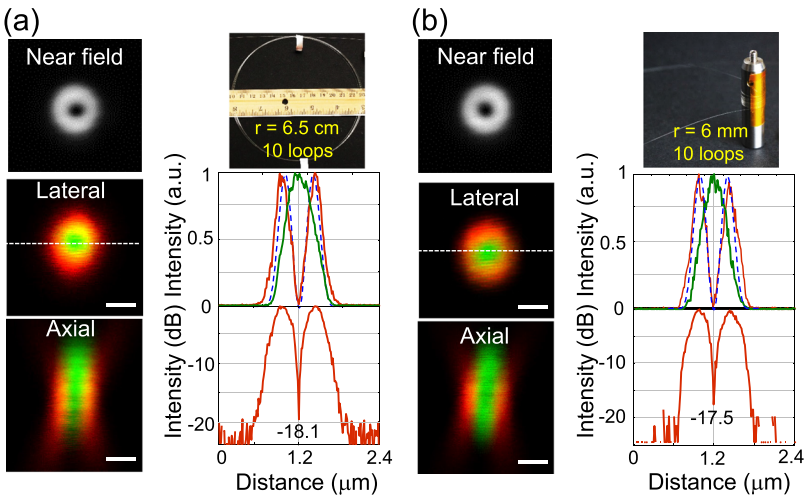

FIG. 5. Experimentally measured near-field mode images and point spread function profiles in the lateral and axial directions for vortex fiber with bending radii of (a) 6.5 cm (10 loops) and (b) 0.6 cm (10 loops). Line-cut profiles of the excitation and the STED beams in linear scale (middle panels) are along dashed lines depicted in the lateral planes of PSF images. The results match with simulations (blue dashed lines). STED beam profiles also plotted in dB scale (bottom panels) to elucidate the extinction ratio. Scale bar: 500 nm.

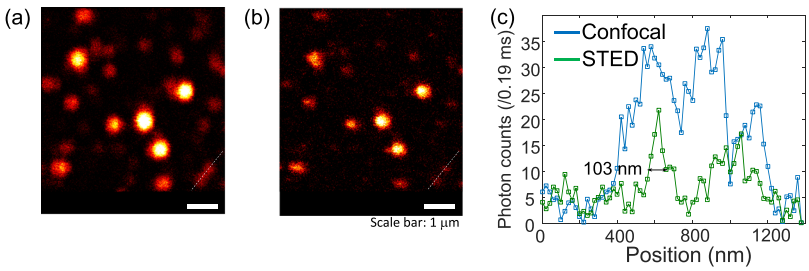

FIG. 6. Images of the dark red fluorescent beads of 40 nm in diameter. Raw data of (a) confocal and (b) subsequential recorded STED images. (c) Line-cut profiles along the white dashed lines in (a) and (b) show an ~4-fold resolution improvement. Scale bar: 1 μm.

sample. The linecut profiles along the white dashed lines in Figs. 6(a) and 6(b) are plotted in Fig. 6(c). The spot size (FWHM) is measured to be 390 nm and 103 nm under the confocal and STED modes, respectively. Although the non-diffraction limited performance of our confocal imaging setup is due to the fact that our excitation beam is not perfect Gaussian, the STED resolution in the lateral direction corresponds to a ~4-fold improvement.

It is worth noting that the resolution improvement is more prominent for dimmer beads primarily because they are single isolated beads, whereas brighter and larger spots are likely to be aggregated bead clusters. The CW STED laser power was limited in our experiment which significantly prevented us from obtaining further resolution improvement. We also notice that when only the STED beam is incident on to the sample, a weak signal from the beads, approximately 2% of that obtained under the confocal mode, is observed, which suggests that the dye is not optimized for operating at this particular STED wavelength. Nevertheless, this experiment is a proof-of-concept demonstration of the fact that STED-base resolution enhancement is achievable with flexible all-fiber devices.

In summary, we demonstrate an all-fiber compact STED microscopy system with vortex fiber modes that is low loss and tolerant to perturbations. We obtain naturally self-aligned PSFs for excitation and depletion beams with sizes and extinction ratios comparable to those obtained with free-space implementations. The fiber we employed can be easily cleaved and spliced with relatively low insertion losses and is compatible with various termination options. While we employed a STED wavelength of 776 nm to validate the performance of our fiber device, the design also ensures that it can be used at shorter wavelengths, thereby offering compatibility with a majority of STED dyes in use today.[30] Likewise, we employed UV-inscribed fiber gratings to realize mode conversion in highly compact (3.1 cm) devices, but this fiber is also suitable for use with other mode conversion schemes that are wavelength tunable in nature. We observe 103-nm lateral resolution using our all-fiber STED microscope, corresponding to ~4-fold improvement compared to a confocal measurement using the same system. While our current demonstration shows the feasibility of performing STED microscopy with vortex fibers, future work would involve the collection of fluorescence with the same fiber, as has been implemented for fiber based multiphoton microscopy,[31] thereby yielding a STED microscope that could potentially lead to endoscopic implementations of this super-resolution technique.

We thank G. Tearney and E. Auksorius for helpful discussions on the microscopy setup, M. Pedersen for helping with the modesolver, T. Morgus and E. Geoffrion for generously loaning optical components, and M. Grogan for help with fiber taper fabrication. This work was supported by NSF (ECCS-1610190) and ONR-MURI (Grant No. N00014-13-1-0627).

REFERENCES

[1]S. W. Hell and J. Wichmann, "Breaking the diffraction resolution limit by stimulated emission: STED fluorescence microscopy," Opt. Lett. **19**, 780 (1994).
[2]Q. Zhan, "Cylindrical vector beams: From mathematical concepts to applications," Adv. Opt. Photonics **1**, 1 (2009).
[3]C. Eggeling, K. I. Willig, S. J. Sahl, and S. W. Hell, "Lens-based fluorescence nanoscopy," Q. Rev. Biophys. **48**(02), 178–243 (2015).
[4]K. I. Willig, R. R. Kellner, R. Medda, B. Hein, S. Jakobs, and S. W. Hell, "Nanoscale resolution in GFP-based microscopy," Nat. Methods **3**, 721 (2006).
[5]E. Rittweger, K. Y. Han, S. E. Irvine, C. Eggeling, and S. W. Hell, "STED microscopy reveals crystal colour centres with nanometric resolution," Nat. Photonics **3**, 144 (2009).
[6]M. Reuss, J. Engelhardt, and S. W. Hell, "Birefringent device converts a standard scanning microscope into a STED microscope," Opt. Express **18**, 1049 (2010).
[7]L. Yan, P. Gregg, E. Karimi, A. Rubano, L. Marrucci, R. Boyd, and S. Ramachandran, "Q-plate enabled spectrally diverse orbital-angular-momentum conversion for STED microscopy," Optica **2**, 900 (2015).
[8]F. Balzarotti, Y. Eilers, K. C. Gwosch, A. H. Gynnå, V. Westphal, F. D. Stefani, J. Elf, and S. W. Hell, "Nanometer resolution imaging and tracking of fluorescent molecules with minimal photon fluxes," Science **355**, 606–612 (2017).
[9]T. Čižmár and K. Dholakia, "Exploiting multimode waveguides for pure fibre-based imaging," Nat. Commun. **3**, 1027 (2012).
[10]L. Yan, E. Auksorius, N. Bozinovic, G. J. Tearney, and S. Ramachandran, "Optical fiber vortices for STED nanoscopy," in CLEO, 2013, paper CTu3N.2.
[11]J. Carpenter, B. J. Eggleton, and J. Schröder, "110 × 110 optical mode transfer matrix inversion," Opt. Express **22**, 96 (2014).
[12]M. Gu, H. Kang, and X. Li, "Breaking the diffraction-limited resolution barrier in fiber-optical two-photon fluorescence endoscopy by an azimuthally-polarized beam," Sci. Rep. **4**, 3627 (2014).
[13]B. M. Heffernan, S. A. Meyer, D. Restrepo, M. E. Siemens, E. A. Gibson, and J. T. Gopinath, "Stimulated emission depletion microscopy with polarization-maintaining fiber," in CLEO, 2018, paper SW4J.3.
[14]S. Ramachandran and P. Kristensen, "Optical vortices in fiber," Nanophotonics **2**(5-6), 455–474 (2013).

[15]S. Ramachandran, P. Kristensen, and M. F. Yan, "Generation and propagation of radially polarized beams in optical fibers," Opt. Lett. **34**(16), 2525–2527 (2009).
[16]C. Brunet, P. Vaity, Y. Messaddeq, S. LaRochelle, and L. A. Rusch, "Design, fabrication and validation of an OAM fiber supporting 36 states," Opt. Express **22**, 26117–26127 (2014).
[17]G. K. L. Wong, M. S. Kang, H. W. Lee, F. Biancalana, C. Conti, T. Weiss, and P. S. J. Russell, "Excitation of orbital angular momentum resonances in helically twisted photonic crystal fiber," Science **337**, 446–449 (2012).
[18]P. Gregg, P. Kristensen, and S. Ramachandran, "Conservation of orbital angular momentum in air-core optical fibers," Optica **2**, 267–270 (2015).
[19]N. Bozinovic, Y. Yue, Y. Ren, M. Tur, P. Kristensen, H. Huang, A. E. Willner, and S. Ramachandran, "Terabit-scale orbital angular momentum mode division multiplexing in fibers," Science **340**, 1545–1548 (2013).
[20]M. E. V. Pedersen, P. Kristensen, L. Grüner-Nielsen, and K. Rottwitt, "Impact of the scalar approximation on the prediction of the group velocity dispersion," J. Lightwave Technol. **29**, 3129–3134 (2011).
[21]S. Ramachandran, "Dispersion-tailored few-mode fibers: A versatile platform for in-fiber photonic devices," J. Lightwave Technol. **23**, 3426 (2005).
[22]S. Savin, M. J. F. Digonnet, G. S. Kino, and H. J. Shaw, "Tunable mechanically induced long-period fiber gratings," Opt. Lett. **25**, 710–712 (2000).
[23]D. Song, T. He, L. Yan, and S. Ramachandran, "200 nm tunable acousto-optic fiber grating for OAM mode generation in the visible spectral range," in Conference on Lasers and Electro-Optics, 2017, paper STu4K.2.
[24]C. D. Poole, H. M. Presby, and J. P. Meester, "Two-mode fibre spatial-mode converter using periodic core deformation," Electron. Lett. **30**(17), 1437–1438 (1994).
[25]K. S. Lee and T. Erdogan, "Fiber mode conversion with tilted gratings in an optical fiber," J. Opt. Soc. Am. A **18**, 1176 (2001).
[26]S. Ramachandran, in *Fiber Based Dispersion Compensation* (Springer Science & Business Media, 2007), Chap. 6.
[27]N. Bozinovic, S. Golowich, P. Kristensen, and S. Ramachandran, "Control of orbital angular momentum of light with optical fibers," Opt. Lett. **37**, 2451 (2012).
[28]B. Richards and E. Wolf, "Electromagnetic diffraction in optical systems. II. Structure of the image field in an aplanatic system," Proc. R. Soc. A **253**, 358–379 (1959).
[29]C. M. Lee, C. J. Engelbrecht, T. D. Soper, F. Helmchen, and E. J. Seibel, "Scanning fiber endoscopy with highly flexible, 1 mm catheterscopes for wide-field, full-color imaging," J. Biophotonics **3**, 385 (2010).
[30]See https://nanobiophotonics.mpibpc.mpg.de/dyes/ for information about dyes commonly used in STED microscopy.
[31]G. Liu, K. Kieu, K. F. Wise, and Z. Chen, "Multiphoton microscopy system with a compact fiber-based femtosecond-pulse laser and handheld probe," J. Biophotonics **4**, 34–39 (2011).